ELSEVIER

Physica B 280 (2000) 134–139

PHYSICA B

www.elsevier.com/locate/physb

^{3}He superfluidity in the presence of aerogel

A. Golov[a,1], J.V. Porto[a,2], D.A. Geller[a], N. Mulders[b], G.J. Lawes[a], J.M. Parpia[a,*]

[a]*Laboratory of Atomic and Solid State Physics, Department of Physics, Cornell University, Ithaca, NY 14853, USA*
[b]*Department of Physics and Astronomy, University of Delaware, Newark, DE 19716, USA*

Abstract

Aerogels introduce disorder into the p-wave-paired superfluid ^{3}He and suppress T_c. Quantifiable (by small angle X-ray scattering) differences in the long-range structure of two identical density aerogels are primarily responsible for their different transition temperatures. We also demonstrate that alteration of the short-range correlations by the addition of ^{4}He does not strongly affect T_c. Acoustic measurements of the fast and slow modes of ^{3}He in aerogel are described. These can be used to explore the superfluid component. We also outline future prospects.

Keywords: Aerogel; Helium-3 superfluid; Superfluid density

0. Introduction

A number of experimental [1–6] and theoretical [7–9] investigations followed the discovery of superfluidity of ^{3}He in aerogel — the only system available for the study of disordered p-wave superfluids. The ^{3}He coherence length, ξ_0, can be changed by varying the pressure, allowing the relative length scale of the impurity distribution to be altered without modifying the impurity density or correlations.

The suppression of the superfluid transition shows substantial variation for ^{3}He that fills identical density aerogels [1–3,5,6]. We start by presenting results of X-ray characterization of two aerogel samples which exhibit quantitatively different ^{3}He phase diagrams. Thus structural correlations within the aerogel, which directly affect the spatial correlations of the superfluid order parameter, are very important for determining the behavior of the transition temperature, T_c, and superfluid density, ρ_s. We also discuss the use of ^{4}He to alter the short-range correlations which does not strongly affect T_c. Finally, we outline the use of low-frequency sound to measure ρ_s.

1. Correlated disorder

Aerogel is not random, and since any "impurity" must be able to rigidly support itself, it will have structural correlations. These correlations extend over longer and longer length scales as the impurity is made more dilute. The aerogels used in this study were all "base catalyzed" [10],[3] and had volume concentrations of 2% (98% open).

Small-angle scattering [11] experiments provide information about the structure of aerogels. Particles of SiO_2 with diameters $a \simeq 30$ Å coalesce into a fractally correlated structure that extends up to a concentration-dependent correlation length, ξ_a, on the order of several hundred to a few thousand Å, above which the aerogel appears homogeneous [12]. Below the length scale, a, the scattered intensity arises predominantly from the surface of the particles. These features are illustrated in Fig. 1, where we plot the scattered intensity from two different aerogels (see Ref. [13] for details). The slopes in the

* Corresponding author. Tel.: +1-607-255-6060; fax: +1-607-255-6428.
E-mail address: jeevak@msc.cornell.edu (J.M. Parpia)
[1] Schuster Laboratory, Manchester University, Manchester M13 9PL, UK.
[2] NIST, Gaithersburg MD, USA.

[3] The aerogels were grown under basic conditions as described in Ref. [10].

0921-4526/00/$ - see front matter
PII: S0921-4526(99)01525-2

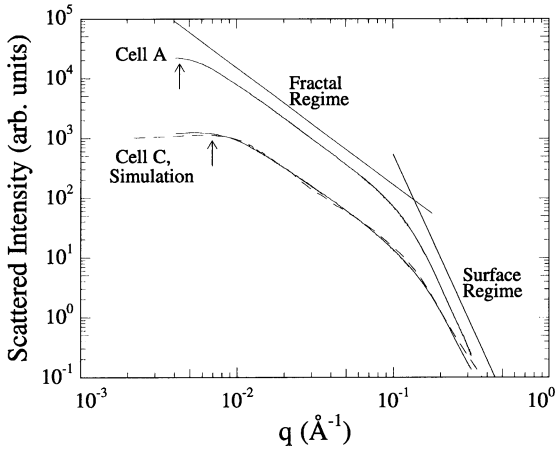

Fig. 1. Small angle X-ray scattering from two aerogels. The upper (lower) solid curve is for the aerogel from cell A (cell C). The dashed line is the scattered intensity calculated for the DLCA model aerogel. The homogeneous regime applies at small q, the fractal regime starts (indicated with the arrows) at $q \simeq 2\pi/\xi_a$. The fractal regime is separated from the surface regime at $q \simeq 2\pi/a$.

Table 1
Five structural parameters for cells A and C

	ξ_a (Å)	a(Å)	K_f	K_s	c
Cell A	1300	$\simeq 30$	-1.91	-5.7	0.02
Cell C	840	28	-1.83	-4.5	0.02

fractal and surface regimes, K_f and K_s, characterize the correlations. The volume concentration, c, gives the average density of SiO_2 but, c alone is inadequate in describing the aerogel. All five parameters for these aerogels are summarized in Table 1.

The DLCA model [11,12] provides a real-space picture of aerogel (Fig. 2). The scattering intensity calculated from the model is also shown in Fig. 1 along with the measured intensities. The agreement for sample C [3] is very good and implies that for that aerogel, the simulation represents the structure between $\simeq 20$ and $\simeq 2500$ Å.

If one looks for the spatial distribution of the superfluid correlations, it is clear that aerogel has no conventional pores with well-defined walls. In fact, if we take the superfluid coherence length, ξ_0, as the shortest length over which the superfluid order parameter can change, there are not any "surfaces" within aerogel along which one can impose diffusive or specular boundary conditions for the spacial variation of the order parameter, since $\xi_0(\simeq 150$–800 Å$) > a(\simeq 30$ Å).

2. Torsional oscillator studies

We examined ^{3}He superfluid in three different aerogel samples using the standard torsion oscillator (TO) technique. The aerogel density fluctuations are small on a scale longer than ξ_0, and the relative contribution of the superfluid component to the moment of inertia due to the tortuosity of its stream lines is less than 0.05 [14] (0.05 being the aerogel tortuosity measured with

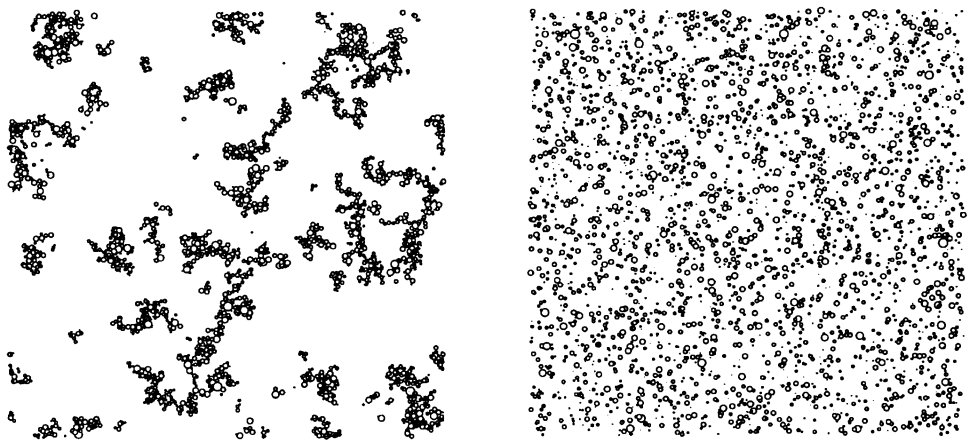

Fig. 2. Panel (a) shows the projection of a 300 Å thick slice of a cube of aerogel, 3500 Å on a side, simulated with the DLCA model. The aerogel has a volume concentration of 0.018. The particle diameters have a Gaussian distribution around 30 Å, with width $\sigma = 15$ Å. For comparison we show in panel (b) a similar slice of the *random* arrangement of spheres with the same diameters and volume fraction.

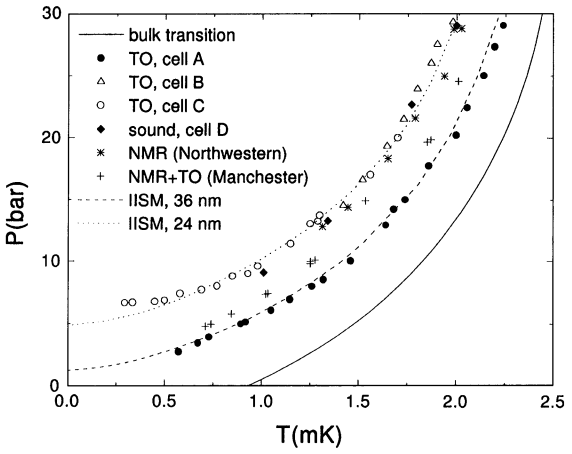

Fig. 3. Transition temperatures, T_c as a function of ^{3}He pressure. The solid line is the bulk transition temperature. The symbols are the results for the samples A, B, C, D as well as for the Northwestern [2] and Manchester [5] samples. The dashed and dotted lines correspond to the calculations using IISM with $L = 36$ and 24 nm, respectively.

superfluid ^{4}He over the whole length scale between $\xi_4 \sim 1$ Å and $\xi_a \sim 1000$ Å). In contrast, the viscous normal fluid contributes its entire moment of inertia. The superfluid density is therefore directly proportional to the period shift, $\Delta P(T)$, through the equation

$$\frac{\rho_s}{\rho} = \frac{\Delta P(T)}{\Delta P_{fill}}. \quad (1)$$

The superfluid transition temperatures in aerogel, T_c, measured in cells A [1], B [14], and C [3] are shown in Fig. 3, along with the results obtained at Northwestern [2] and Manchester [5]. While there is reasonable agreement between samples B, C and the results obtained at Northwestern, it is clear that there are substantial differences between these and the results of sample A, while the Manchester T_c data are intermediate. All five samples had a nominal aerogel volume fraction of 2%, and the quantitative differences clearly indicate that some other property of the aerogel, presumably structural correlations, plays an important role. Scattering measurements from samples A and C represent the extreme values for this aerogel density.

In Fig. 1 and Table 1, there are clear differences in almost all of the characteristic properties of samples A and C. The aerogel in cell A was one of the first samples made and the mass concentration was carefully determined, but the gelling conditions were not documented. We speculate that sample A was catalyzed in a less basic environment than sample C. The largest difference is in the correlation length ξ_a, where we find $\xi_a = 1300$ Å for sample A and $\xi_a = 840$ Å for sample C. These differences help to explain the differences in T_c.

As a first attempt, Thuneberg et al. calculated the suppression of ρ_s and T_c in aerogel neglecting the spatial variations of the (suppressed) ^{3}He order parameter [7]. This approach is justified if there are no fluctuations of the aerogel density on a scale larger than ξ_0. The results failed to account for both the pressure dependence of T_c, and the ρ_s suppression versus T_c suppression. The ρ_s suppression in aerogel is much stronger than that of T_c, which is found to be true for inhomogeneous-order parameters [15]. A more realistic modification [7] models the long-range inhomogeneity of aerogel as a collection of periodically distributed spherical voids with reduced scattering amplitude. This isotropic inhomogeneous scattering model (IISM) nicely fits the experimental values of $T_c(p)$ (Fig. 3). The parameter of this model is the sample-dependent length scale L which is related to the void radius as $R \simeq 5.6L$ for good fit. For the two samples (A and C) the fitting parameters are $L_A = 360$ Å and $L_C = 240$ Å ($R_A \simeq 2000$ Å and $R_C \simeq 1300$ Å). We note that the correlation lengths for those samples, 1300 and 840 Å (Table 1), have the same ratio: $\frac{1300}{840} = 1.55$ and $L_A/L_C = \frac{360}{240} = 1.5$.

3. Modifying the disorder with ^{4}He film

We wanted to modify the distribution of short length scale disorder relative to ξ_0 and examine how T_c and ρ_s are altered. This was achieved by coating the aerogel with a thick ^{4}He film that preferentially fills the smallest pores and thus raises the lower cut-off of the correlations of disorder sampled by the ^{3}He. For details see Refs. [14,16].

We monitored the period of a TO containing sample B. A concentric plate capacitor, inside which the aerogel was grown, allowed us to determine the molar fraction of ^{4}He, x_4 [17]. Considering the ^{3}He–^{4}He mixture as completely phase separated and neglecting the molar volume difference between liquid ^{3}He and ^{4}He, we get

$$\frac{\rho_s}{\rho} = \frac{1}{1 - x_4}\frac{\Delta P(T)}{\Delta P_{fill}}, \quad (2)$$

where the $(1 - x_4)$ term accounts for the ^{3}He volume change due to replacement of ^{3}He by ^{4}He. Our results are summarized in Fig. 4 where we show T_c and ρ_s/ρ at $0.5T_c$ for various x_4 at $p = 21.6$ bar. With addition of ^{4}He, we observed a slight increase in T_c while ρ_s/ρ decreased substantially.

When x_4 is increased from zero, a thin van der Waals film of ^{4}He coexists with capillary condensed ^{4}He filling the smallest pores. Upon adding ^{4}He, successively larger pores are filled with the ^{4}He. Eventually, only the thick ^{4}He film capillary condenses around the regions rich in silica, leaving the ^{3}He phase in the center of the biggest voids, thus altering the structure of the medium sampled

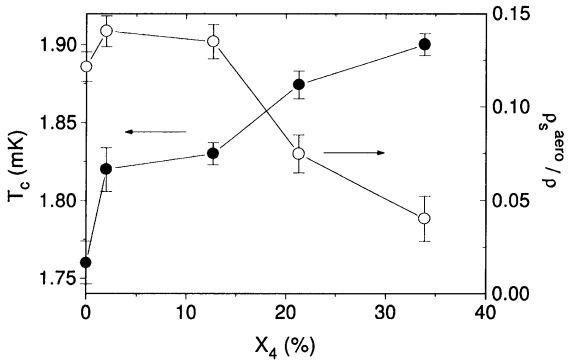

Fig. 4. T_c (●, left axis) and ρ_s/ρ at $T = 0.5T_c$ (○, right axis) versus x_4. The lines connect the data points.

by the ^{3}He superfluid. At some $x_4 = x_c \sim 30\%$, the regions of ^{3}He get completely encapsulated by the ^{4}He-rich phase and thus isolated into islands. Hence, the ^{3}He superflow can be suppressed even though the local Cooper pairing is still strong. This picture is consistent with our observation that T_c is not suppressed further by the addition of ^{4}He, but that the ρ_s is. The decrease in ρ_s could be attributed to weakened phase coherence between the more open regions.

The observed enhancement of T_c accompanied by the reduction of ρ_s is inconsistent with the homogeneous scattering model that describes the disorder by a single parameter, the mean free path. The IISM model [7], that incorporates periodic voids into aerogel, is more realistic. Due to the proximity effect, it produces a single T_c for the sample as a whole. However, the weight of the strongly scattering regions in the determination of T_c is exponentially small compared to that of weak scattering regions. This result is in agreement with our finding that T_c slightly increased after the strongly scattering regions are filled with ^{4}He.

While T_c of pure ^{3}He is very dependent on the porosity of aerogel in the range 99.5–98% [5,18], and even on the particular distribution of correlations at the same porosity, it virtually is not altered with the addition of up to 34% ^{4}He which effectively decreases the volume available for ^{3}He from 98% to 64%. By changing the aerogel's density or microscopic structure one can affect the long-range cut-off of the correlations of the disorder, ξ_a. On the other hand, adding ^{4}He affects only the short-range correlations leaving the biggest voids unchanged.

4. Acoustic properties

A porous material filled with superfluid helium simultaneously possesses the properties of elastic solid and superfluid liquid. The acoustic properties of such a system were outlined in connection with the hypothetical "supersolid" [19,20]: it has to have three solid-like and one critical fourth-sound-like modes. In typical porous media, the normal component of ^{3}He is viscously clamped to the porous matrix while the superfluid component is free to move. Very open aerogels are special among the other materials because their own sound velocities are smaller than that of liquid helium. The solid-like modes are the oscillations of the matrix together with the normal component of ^{3}He: one longitudinal and two transverse sounds. The critical liquid-like mode is the out-of-phase oscillation of the superfluid component and the matrix (aerogel together with the normal component). The latter holds both pressure and temperature waves and is well-suited for experimental determination of ρ_s/ρ.

To find the longitudinal solutions, McKenna et al. [21] combined the two-fluid hydrodynamics with the elasticity of an isotropic matrix that yields the equation for the velocities of both longitudinal sounds, $c_x = (c_f, c_s)$ (fast, c_f, and slow, c_s):

$$(c_x^2 - c_1^2)(c_x^2 - c_2^2) + \frac{\rho_a}{\rho_n}(c_x^2 - c_a^2)(c_x^2 - c_4^2) = 0, \tag{3}$$

where c_1, c_2, c_4, c_a are the first, second, fourth and empty aerogel speeds of sound, respectively.

Our resonator consisted of a cylinder of aerogel (sample D), grown under the same conditions as sample C. Piezoceramic transducers were pressed against the ends of the cylinder and spectra were recorded as the quadrature response of the microphone to the oscillations of the speaker while the drive frequency was swept continuously. For details see Refs. [22,23].

The evolution with temperature of the fundamental resonance of the fast mode is shown in (Fig. 5). The sound velocity, c_f, is 80% of the bulk ^{3}He first sound velocity. In the superfluid phase, c_f changes by only $\sim 1\%$ or less. Because $c_2^2 \ll c_f^2$ and $c_a^2 \ll c_f^2$ the solution of Eq. (3) is given by

$$c_f^2 \approx c_1^2\left(1 + \frac{\rho_a}{\rho}\frac{\rho_s(T)}{\rho_n(T)}\right)\Big/\left(1 + \frac{\rho_a}{\rho_n(T)}\right). \tag{4}$$

The aerogel contributes little to the restoring force, which is dominated by the compressibility of the helium, and only adds its mass, producing a decrease in the sound speed.

The slow mode is an oscillation of a deformation of the aerogel combined with a simultaneous out-of-phase motion of the superfluid component. Thanks to the validity of the inequalities, $c_2^2 \ll c_s^2 \ll c_a^2 \ll c_1^2$, Eq. (3) takes the form

$$c_s^2 = c_a^2 \frac{\rho_a}{\rho}\frac{\rho_s(T)}{\rho}. \tag{5}$$

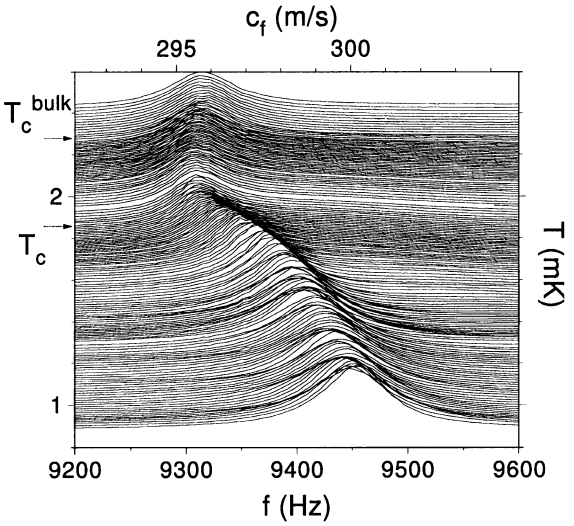

Fig. 5. Fundamental resonances of the fast mode ($p = 21.7$ bar) offset vertically with temperature.

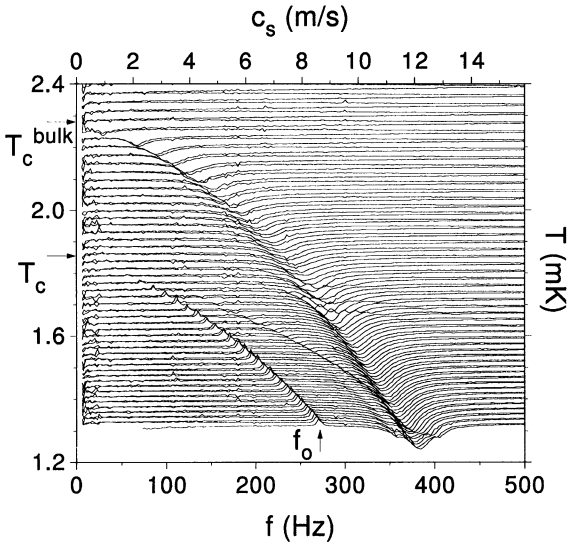

Fig. 6. Spectra of the slow mode ($p = 21.7$ bar) off-set vertically with temperature. The sharp positive peak (f_0) disappearing at $T_c = 1.85$ mK is the fundamental slow mode resonance. The strong broad dip vanishing at $T_c^{bulk} = 2.28$ mK is the Helmholtz resonance. Five higher modes with the same T_c are also shown (two cross the Helmholtz mode at 1.2 and 1.4 mK and three rapidly changing modes cross just below T_c).

Using Eq. (5) ρ_s/ρ can be determined from the measured ratio of sound velocities, c_s/c_a. In our experiment $c_a \approx 51$ m/s.

The slow mode resonances at different temperatures are shown in Fig. 6. The transition temperatures, $T_c(p)$, are in good agreement with those from sample C over the range $p = 9$–29 bar (Fig. 3).

5. Summary

We have seen that the density alone is insufficient to characterize an aerogel, at least as far as the properties of ^{3}He are concerned. We have concentrated our discussion on hydrodynamic studies of ^{3}He in aerogel. These are important tools for detecting the superfluidity of the system and the extent of its suppression by disorder. There are many aspects that will prove to be interesting to study in the future, including the question of the dominant low-field phase of the superfluid [24,25]. At sufficiently low density of aerogel the ^{3}He properties should converge with those of bulk ^{3}He; it is thus important to study the phase diagram for aerogel densities less than 1% [18]. Further acoustic studies are needed, not only because it is an accurate tool of measuring ρ_s/ρ, but also because sound dissipation could yield important answers about mutual friction, etc. The transverse sound in this system has yet to be observed. Finally, the studies of superfluid ^{3}He–^{4}He mixtures in aerogel should be promising, both at low and high ^{4}He concentrations. Here ^{4}He can play a role of thin or thick films which either modify the strength of magnetic scattering or short-range morphology of the aerogel. The hydrodynamics of two coupled superfluids, ^{4}He and ^{3}He, is also of great interest [26,27].

Acknowledgements

Support of the NSF through DMR-9705295 is acknowledged. Samples provided to Cornell, Manchester and Northwestern were grown at Penn State.

References

[1] J.V. Porto, J.M. Parpia, Phys. Rev. Lett. 74 (1995) 4667.
[2] D.T. Sprague, T.M. Haard, J.B. Kycia, M.R. Rand, Y. Lee, P.J. Hamot, W. P. Halperin, Phys. Rev. Lett. 75 (1995) 661.
[3] K. Matsumoto, J.V. Porto, L. Pollack, T.L. Ho, J.M. Parpia, Phys. Rev. Lett. 79 (1997) 253.
[4] D.T. Sprague, T.M. Haard, J.B. Kycia, M.R. Rand, Y. Lee, P.J. Hamot, W.P. Halperin, Phys. Rev. Lett. 77 (1996) 4568.
[5] H. Alles, J.J. Kaplinsky, P.S. Wootton, J.D. Reppy, J.R. Hook, Physica B (Amsterdam) 255 (1998) 1.
[6] B.I. Barker, L. Polukhina, J.F. Poco, L.W. Hrubesh, D.D. Osheroff, J. Low-Temp. Phys. 113 (1998) 635.
[7] E.V. Thuneberg, S.K. Yip, M. Fogelstrom, J.A. Sauls, Phys. Rev. Lett. 80 (1998) 2861.
[8] G.E. Volovik, Pis'ma Zh. Eksp. Teor. Fiz. 63 (1996) 281 [JETP Lett. 63 (1996) 301].

[9] V.P. Mineev, Pis'ma Zh. Eksp. Teor. Fiz. 66 (1997) 655 [JETP Lett. 66 (1997) 693].
[10] T.M. Tillotson, L.W. Hrubesh, J. Non-Cryst. Solids. 145 (1992) 44.
[11] A. Hasmy, E. Anglaret, M. Foret, J. Pelous, R. Jullien, Phys. Rev. B 50 (1994) 6006.
[12] A. Hasmy, R. Vacher, R. Jullien, Phys. Rev. B 50 (1994) 1305.
[13] J.V. Porto, J.M. Parpia, Phys. Rev. B 59 (1999) 14583.
[14] A. Golov, J.V. Porto, J.M. Parpia, Phys. Rev. Lett. 80 (1998) 4486.
[15] M. Franz, C. Kallin, A.J. Berlinsky, M.I. Salkola, Phys. Rev. B 56 (1997) 7882.
[16] A. Golov, J.V. Porto, J.M. Parpia, J. Low-Temp. Phys. 113 (1998) 329.
[17] A. Golov, J.V. Porto, J.M. Parpia, J. Low-Temp. Phys. 110 (1998) 591.
[18] G.J. Lawes, S.C.J. Kingsley, N. Mulders, J.R. Beamish, J.M. Parpia, Physica B (2000), these Proceedings.
[19] A.F. Andreev, I.M. Lifshitz, Zh. Eksp. Teor. Fiz. 56 (1969) 2057 [Sov. Phys. JETP 29 (1969) 1107].
[20] M. Liu, Phys. Rev. B 18 (1978) 1165.
[21] M.J. McKenna, T. Slawecki, J.D. Maynard, Phys. Rev. Lett. 66 (1991) 1878.
[22] D.A. Geller, A. Golov, N. Mulders, M.H.W. Chan, J.M. Parpia, J. Low-Temp. Phys. 113 (1998) 339.
[23] A. Golov, D.A. Geller, J.M. Parpia, N. Mulders, Phys. Rev. Lett. 82 (1999) 3492.
[24] H. Alles, J. Kaplinsky, P.S. Wootton, J.D. Reppy, J.H. Naish, J.R. Hook, Phys. Rev. Lett. (1999) to appear.
[25] J. Hook, H. Alles, J. Kaplinsky, J. Naish, P. Wootton, Physica B (2000), these Proceedings.
[26] G.E. Volovik, private communication.
[27] A.F. Andreev, E. Bashkin, Zh. Eksp. Teor. Fiz. 69 (1975) 319 [Sov. Phys. JETP 42 (1976) 164].